Pore Pressure Responses of Liquefied Numerical Sand Columns

Widjojo A. Prakoso*, Dheyaini Mazaya, Rumaisha A. Kartika
Department of Civil and Environmental Engineering, Universitas Indonesia, Depok, INDONESIA
Kampus UI, Depok 16424
*Corresponding authors: wprakoso@eng.ui.ac.id

ABSTRACT The Palu 28 September 2021 M 7.5 Earthquake, followed by a series of aftershocks within a short time frame, has brought several new challenges to the understanding of liquefaction and its associated geotechnical phenomena. The common geotechnical conditions of the Palu area include layered soil conditions and thin soil with lower permeability. This research determined the dynamic effective stress analysis (ESA) of four different liquefiable layered sand columns and explicitly modeled the layered soils, variability, and aftershocks conditions. The dynamic ESA employed the PM4Sand constitutive model for liquefiable sands, implemented in the OpenSees platform. Furthermore, three ground motion sets, namely "main shock only", "mainshock plus aftershock", and "aftershock only" of variable amplitude, as well as single-frequency harmonic motions, were used to conduct this research. The models were validated by comparing their results against laboratory tests and field measurements. The saturated sand layers in all cases subjected to "main shock only" were liquefied with different detailed excess pore pressure (EPP) responses, highlighting the importance of the system response of liquefying sand columns. The cases subjected to "main shock plus aftershock" showed a much longer, higher EPP state, while cases subjected to both "main shock plus aftershock" and "aftershock only" indicated a longer liquefaction state during the aftershock. The implication of the longer duration in the higher EPP and the longer liquefaction states is the possible existence of prolonged lower shear strength conditions. The different EPP responses from varying geotechnical conditions represented by the four sand columns suggested that the variability of geotechnical conditions is likely to influence the system response.

KEYWORDS Palu Earthquake; Liquefaction; Layered Soils; Ground Motions; Dynamic Effective Stress Analysis.

1 INTRODUCTION

The Palu M 7.5 Earthquake that occurred on 28 September 2021 has led to several new challenges related to liquefaction and its geotechnical phenomena (Gallant *et al.,* 2020, Mason *et al.,* 2021). These challenges were addressed in studies by Harninto and Prakoso (2020); Ramdhiani and Prakoso (2020); Rahayu *et al.,* (2020a; 2020b); and Prakoso (2021). At a macro level, this research is an aspect of a broader earthquake geotechnical engineering program implemented in Central Sulawesi (Pramono *et al.,* 2017; 2020).

This research is focused on understanding the liquefaction mechanism of layered soils. It is important to note that geotechnical investigations carried out in Palu stated that layered soils were common in this area (Rahayu *et al.,* 2020a; 2020b). Additionally, a thin soil layer with low permeability has been hypothesized to significantly affect the observed phenomenon (Harninto and Prakoso, 2020). Dynamic effective stress analysis (ESA) has

recently been extensively used to resolve the research problem (Cubrinovski *et al.,* 2019; Hutabarat and Bray 2021a; 2021b). The liquefaction mechanism of layered soils, including sand columns, has also undergone laboratory tests (Kokusho and Kojima 2002). An increase in pore pressure and subsequent dissipation depends on the soil layers. All these indicate that the liquefaction mechanism is complex and requires a more detailed analysis than typical simplified approaches (Youd *et al.*, 2001). Phoon *et al.,* (2016) stated that it is interesting to examine the effect of geotechnical variabilities on this mechanism.

The main shock of the Palu Earthquake was followed by five significant aftershocks within less than one hour (Prakoso, 2021). It has been proven by field measurements that these could prolong the liquefaction state of a sand layer (Unjoh, 2012).

This research employed the numerical analysis of liquefied one-dimensional layered sand columns and the dynamic ESA to examine earlier

identified conditions. Different sand columns and layers were examined to assess the effects of soil layering and associated geotechnical variabilities on pore pressure development and subsequent dissipation. However, various ground motions consisting of main and aftershocks were used to assess the impact of a series of earthquakes on the pore pressure. The possible combination of these effects was further examined and discussed.

2 ANALYTICAL METHOD

2.1 Basic Approach

A series of one-dimensional liquefaction numerical tests were carried out to discern the behavior of saturated layered sands. This research adopted the basic experimental design proposed by Kokusho and Kojima (2002). The one-dimensional sand layers were liquefied by variable amplitude and single frequency harmonic motions. Additionally, excess pore pressures during and after the entire process were recorded at different levels.

This study used two basic types of layered sand columns with a height of 2 m. The first, known as Cases 1A and 1B, consisted of 900 mm upper (D_R = 30%), a 50 mm medium dense (D_R = 48%), and a 950 mm lower sand layers (D_R = 44%). This basic type was then varied in the coefficient of permeability of the top sand layer, with Cases 1A and B consisting of 10^{-4} m/s and 10^{-5} m/s, respectively.

According to Andersen and Schjetne (2013), the reason behind this was to determine the variability of the coefficient of permeability of sands. The second basic type, Cases 2A, and 2B consisted of 1,000 mm upper (D_R = 40%) and overlying 900 mm lower sand layers (D_R = 37%). This varied with the depth of the groundwater table, taking into account its natural fluctuation at a depth of 500 mm. The 100 mm bottom soil layer was assumed to be elastic gravel and all the cases considered are shown in Figure 1.
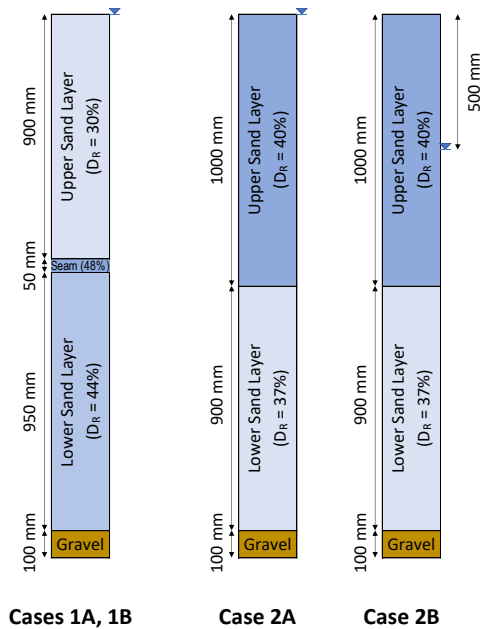

Figure 1. Four sand columns considered

The recorded outputs were primarily the excess pore pressure responses at different depths. These were further analyzed to determine their ratio:

$$r_u = \Delta u / \sigma'_{v0} \qquad (1)$$

where Δu is excess pore pressure and σ'_{v0} is initial vertical effective stress. According to Hutabarat and Bray (2021a; 2021b) liquefaction is expected when a value is 0.9 or greater.

2.2 Soil Parameters

The hypothetical soil materials were modeled using PM4Sand (Boulanger and Ziotopoulou, 2017), shown in Table 1, alongside its primary parameters. Based on the critical state concept and bounding surface plasticity theory, this effective stress model is also used to simulate the sand contractive–dilative response under cyclic shearing conditions. Regarding the primary parameters of PM4Sand, this study defined only the relative density D_R, while the shear modulus coefficient G_o and the number of cycles required to reach liquefaction represented by the contraction rate parameter h_{po} was subsequently determined using the procedure proposed by Boulanger and Ziotopoulou (2017).

Table 1. Parameters for PM4Sand

Parameter	Case 1				Case 2	
	Upper 1A	Upper 1B	Seam	Lower	Upper	Lower
Relative Density, D_R (%)	30		48	44	40	37
Unit Weight, γ (kN/m^3)	19.6		19.9	19.8	20.4	19.6
Permeability (m/s)	10^{-4}	10^{-5}	10^{-5}	10^{-4}	10^{-5}	10^{-4}
Shear modulus coefficient, G_o	430		604	564	524	495
Contraction rate parameter, h_{po}	0.36		0.55	0.39	0.38	0.32
Void Ratio, e	0.71		0.66	0.67	0.68	0.70

Meanwhile, other necessary parameters were determined based on correlations available in standard textbooks. The 100 mm bottom soil was assumed to be elastic with a shear wave velocity of 450 m/s.

2.3 Input Motion

The input motions include a variable amplitude and a single harmonic velocity of 4 Hz. The three motions utilized are GM1 which lasted for 3 seconds from 5 s to 8 s (12 cycles), while GM3 lasted for 2 seconds from 15 s to 17 s (8 cycles). Additionally, GM2 is a combination of GM1 and GM3. The peak motion velocities were 0.12 m/s and 0.06 m/s for GM1 and GM3, respectively. Figure 2 shows the harmonic velocity time history for GM2, and it was further highlighted that GM1 and GM3 represented the main and aftershocks, respectively. GM2 represented the main shock, followed by an aftershock with a time step of 0.005 s. The input motions were applied at the model base.

2.4 Finite Element Model

The dynamic nonlinear effective stress analysis (ESA) was carried out using OpenSees version 3.0. The ESA model employed was developed by Hutabarat and Bray (2021a, 2021b). Some important features were highlighted as follows

the u-p formulation consisting of u as displacement of soil phase and p as fluid pore pressure developed by Zienkiewicz and Shiomi was implemented in the plane strain four-node quadrilateral elements and used to solve the solid-fluid equilibrium and mass balance governing equations. The displacement of the solid phase and the fluid pore pressure was resolved at the element corner nodes, while the stress and strain were subsequently computed at the center point of each element.

The sand columns were modeled using forty 50 mm thick, four-node quadrilateral elements. In terms of modelling one-dimensional (1D) sand columns with a simple shear mechanism, the nodes at the same elevations were assumed to have similar horizontal displacement. The model base was fixed against any vertical displacement. The pore pressure boundary conditions were zero for nodes above the groundwater table and free for the saturated ones. The Lyster and Kuhlemeyer dashpot was used at the base of the model. The damping matrix was based on the Rayleigh formulation, with a critical ratio of 2%.

The time-step selected for the dynamic analysis was 0.001 s for 40 s during its simulation, while that of advection was 0.01 s to speed up the computation
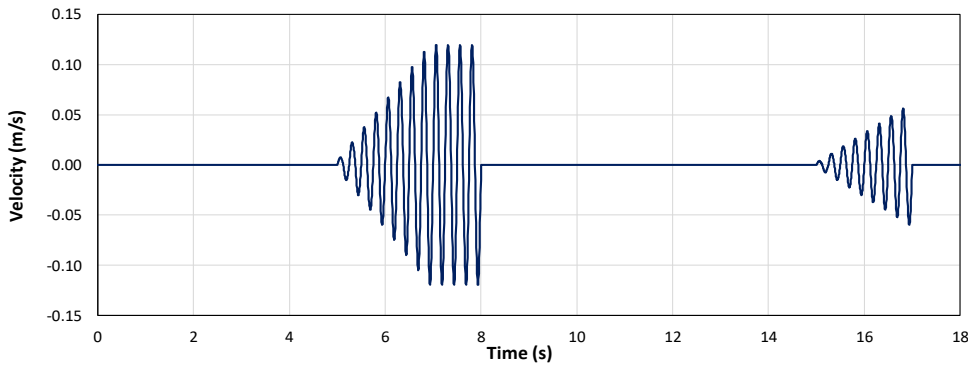
Figure 2. Input velocity for GM2

3   RESULTS

3.1   Cases 1A and 1B

The time histories of excess pore pressure ratio r_u for Cases 1A and 1B subjected to GM1 are shown in Figures 3 and 4, respectively. Figures 3a and 4a show the overall responses at six different depths, while 3b and 4b indicate the time-specific responses at selected depths. The responses of r_u in both cases started immediately after the initiation of ground motion at 5 s and leveled off before 6 s with a ground motion to level off at 7 s. The r_u after the ground motion ended at 8 s and varied from the various cases. For Case 1A, with a higher coefficient of permeability for the upper sand layer, r_u decreased immediately after 8 s and simultaneously for all depths. However, for Case 1B, with a lower coefficient of permeability for the upper sand layer, the responses were significantly much slower than those for Case 1A, and r_u remained relatively high for a rather long time after the ground motion ended. Furthermore, the responses also varied for different depths where r_u of deeper observation points decreased faster than the middle ones. The responses of the shallower points increased after the ground motion stopped for approximately 2 s, while r_u decreased.

The distribution of excess pore pressure (EPP) depth for Cases 1A and 1B, including the change with time, is shown in Figure 5. The responses increased rapidly as the ground motion took place. The effect of the 50 mm thick seam at a depth of 0.9 m for Case 1A is observed as EPP in the upper sand layer with a higher coefficient of permeability lower than that of 1B. For Case 1A, EPP decreased rapidly between 8 s and 9.85 s, reaching an average r_u of 0.1. Meanwhile, for Case 1B, at 10 s, EPP in the lower sand layer decreased, although it increased in the upper sand layer, indicating an upward excess pore pressure flow. The decrease in EPP was gradual, reaching an average r_u of 0.1 at 21.5 s after the ground motion was halted.

The time history of r_u for Case 1B subjected to GM2 is shown in Figure 6. The overall responses at six different depths are shown in Figure 6a, while r_u at selected depths for aftershock ground motion started at 15 s and ended at 17 s. It was highlighted that r_u at 15 s was not equivalent to zero as it had not fully been dissipated after the main shock. The general responses r_u due to the aftershock were similar to those as a result of the main one or GM1, and it remained relatively high for a rather long time after the ground motion ended. The responses r_u of deeper observation points decreased faster than the middle ones. Meanwhile, r_u of the shallower points increased after the ground motion ended at approximately 1.5 s, followed by a subsequent decrease.
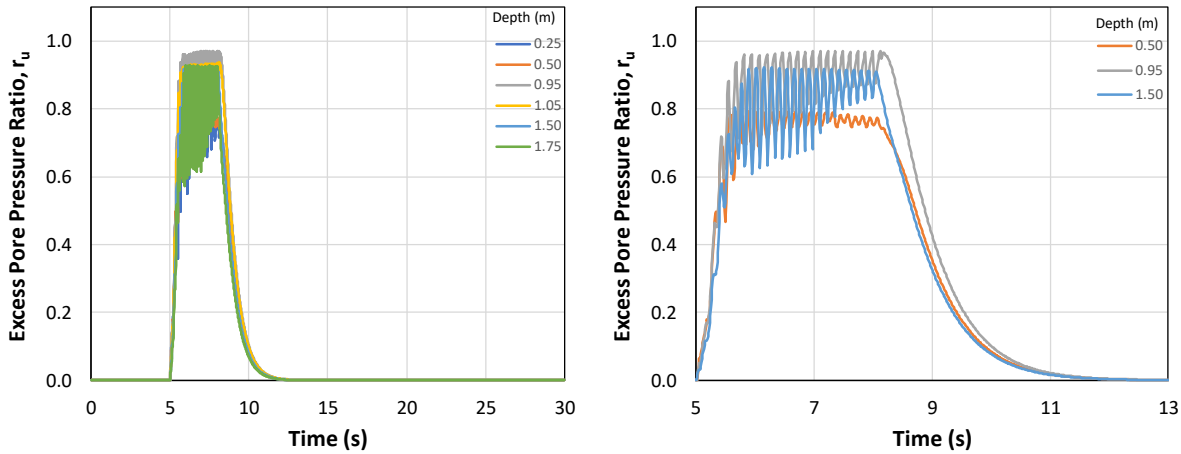
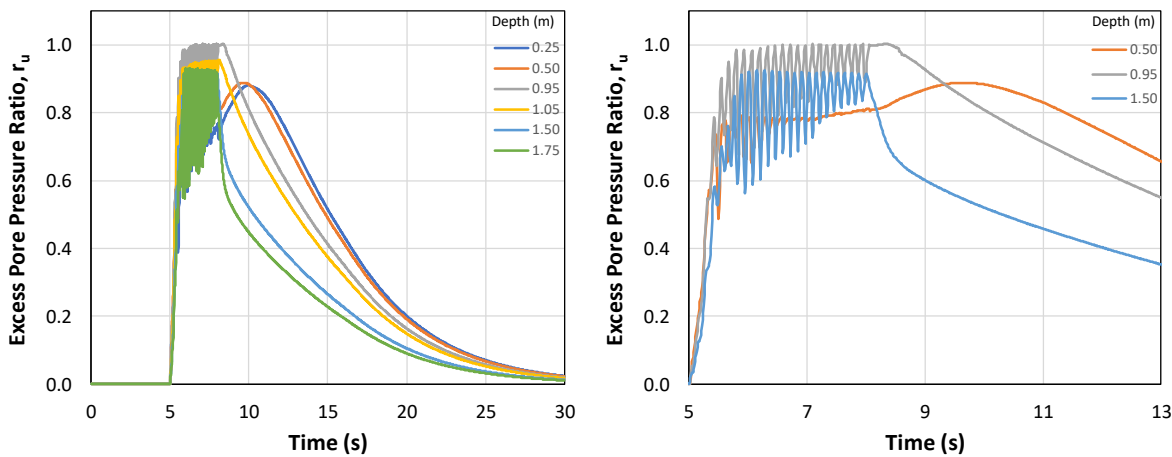Figure 3. Time history of ru for Case 1A subjected to GM1

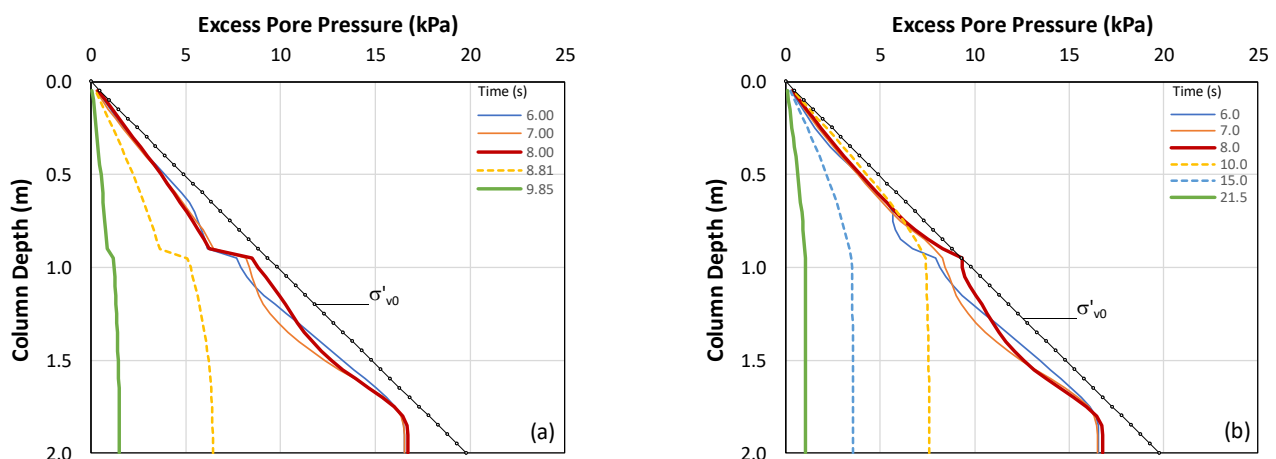Figure 4. Time history of ru for Case 1B subjected to GM1

Figure 5. Distribution with depth of EPP for (a) Case 1A and (b) Case 1B subjected to GM1

The distribution of EPP depth and the change of time is shown in Figure 6c. The average r_un at the start of the aftershock was relatively 0.34, and EPP increased rapidly afterward. At 19 s, EPP in the lower sand layer decreased, although it slightly increased in the upper layer, indicating an upward excess pore pressure flow. The further decrease in EPP was gradual, reaching an average r_u of 0.1 at 30.4 s towards the end of the aftershock.

The distribution of EPP depth and the time change for Case 1B subjected to GM3 is shown in Figure 7a. Comparing Case 1B subjected to GM1 in Figures 7a to 5b, the rate of increase in EPP was perceived as a function of ground motion amplitude. The rise in time at 1s after the start of GM3 at 16 s was less than that of GM1 at 6 s. The comparison between Figures 7a to 6c, such as Case 1B subjected to GM2, indicated that the rate of decrease in EPP after the ground motion ended was quite similar. The average r_u of 0.1 was achieved relatively at the same time. Figure 7b compares the time history of r_u due to GM3 and GM2, and it indicated that the initial r_u at time = 15 s caused its maximum to be reached more quickly, therefore the state of liquefaction tended to be longer.

3.2 Cases 2A and 2B

The time histories of excess pore pressure ratio r_u for Cases 2A and 2B subjected to GM1 are shown in Figures 8 and 9, respectively; The overall responses at several depths are shown in Figures 8a and 9a. Meanwhile, 8b and 9b show the time-specific responses at selected depths. The responses r_u in both cases started immediately after the initiation of ground motion at 5 s and leveled off at 7 s. The r_u after the ground motion ended at 8 s, which tends to vary depending on the groundwater depths. Unlike Case 2A, the lower part of the upper sand layer at a depth of 0.75 m for 2B failed to liquefy.
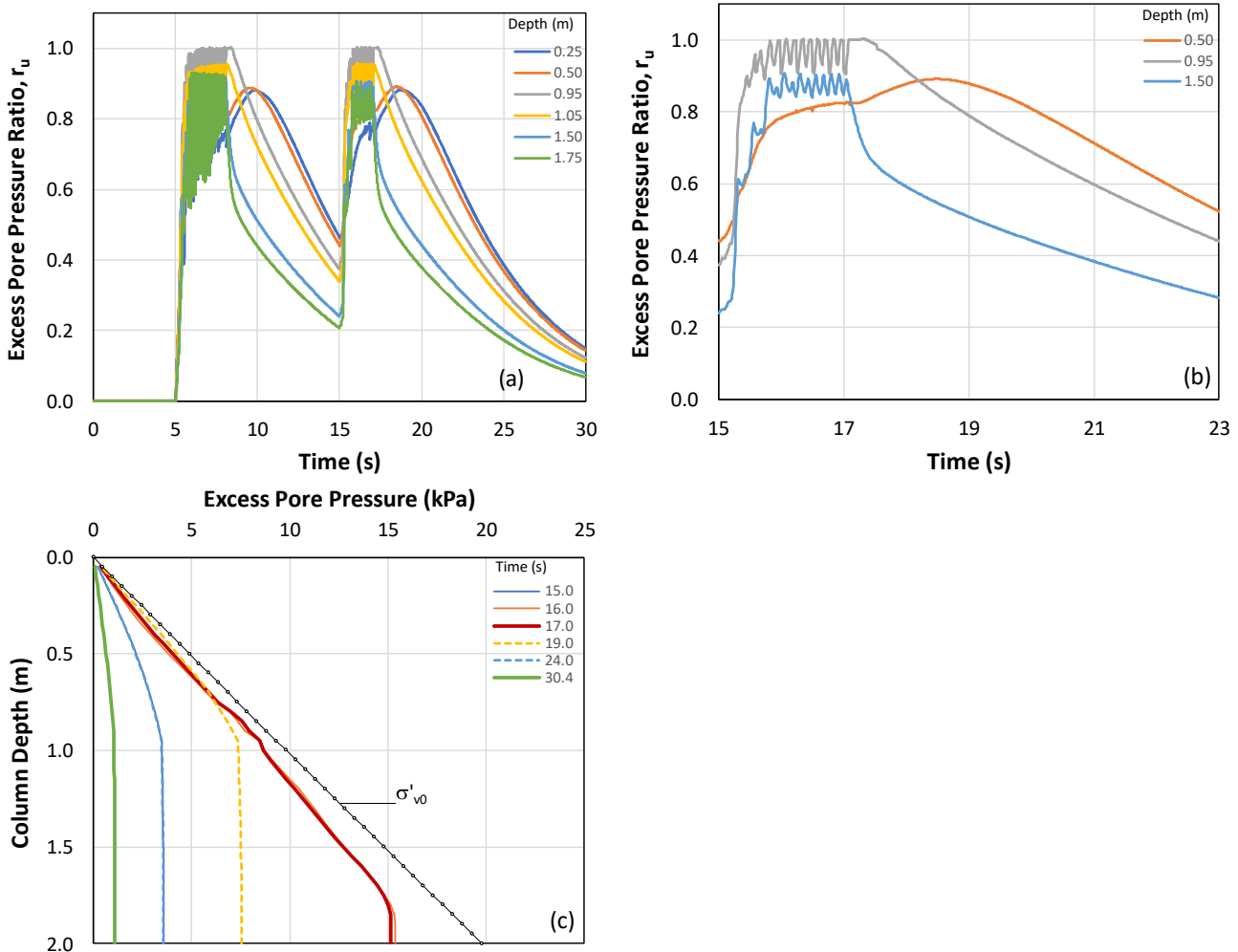

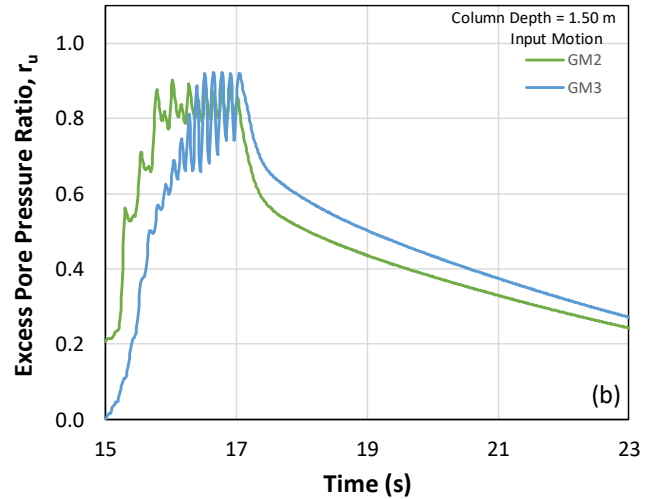Figure 6. Time history of ru and distribution with depth of EPP for Case 1B subjected to GM2
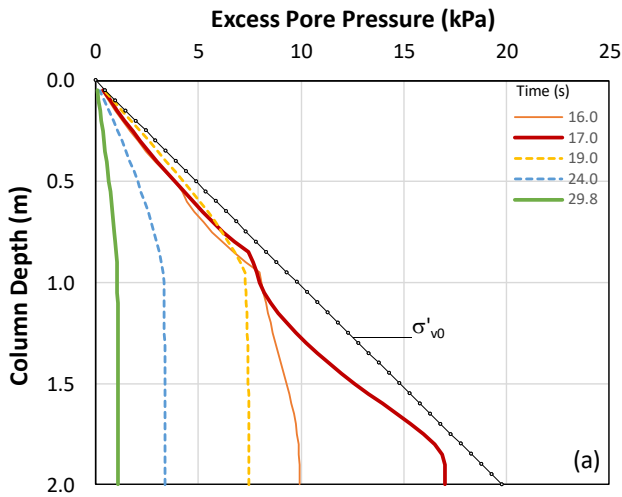
Figure 7. (a) Distribution with depth of EPP for Case 1B subjected to GM3, and (b) time history of ru comparison for smaller ground motion
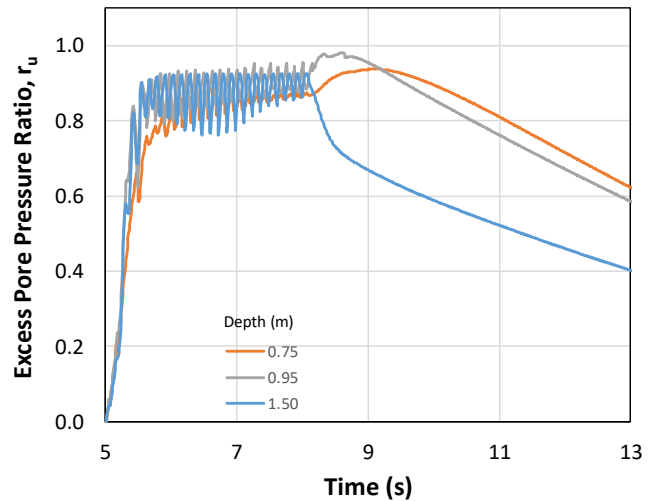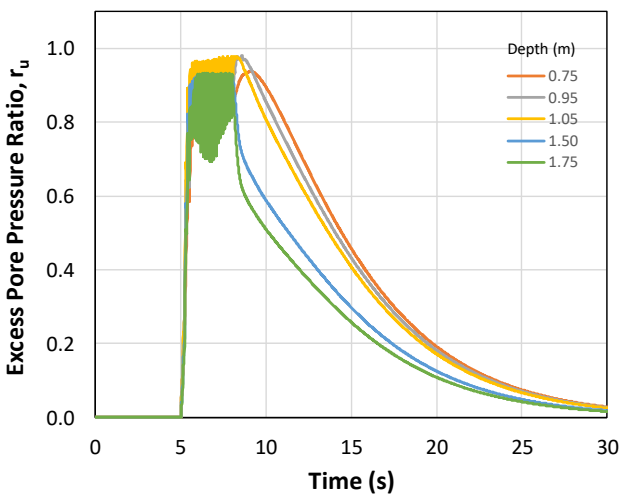

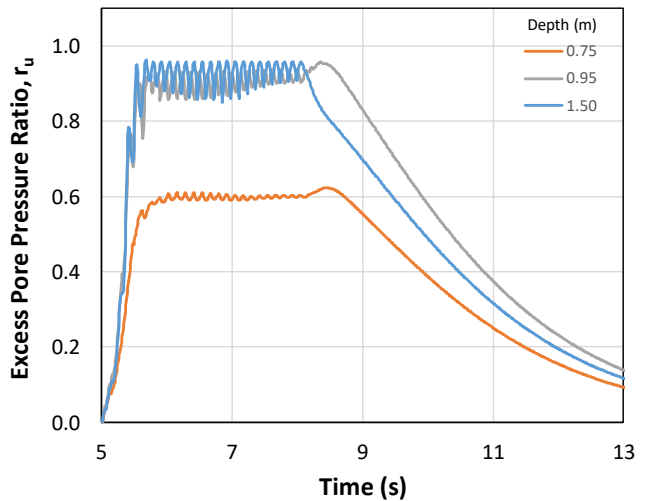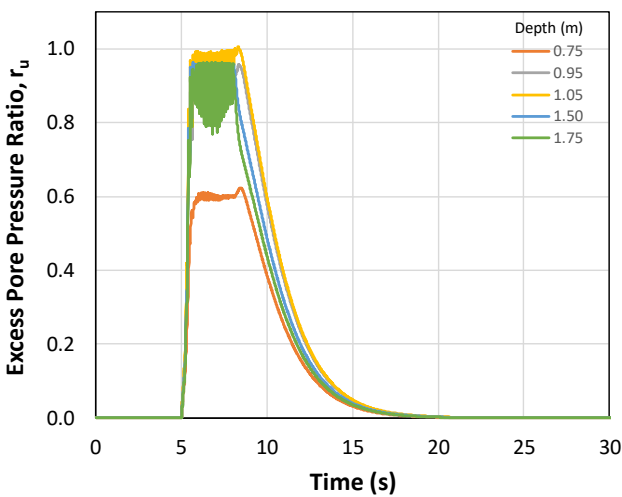Figure 8. Time history of ru for Case 2A subjected to GM1

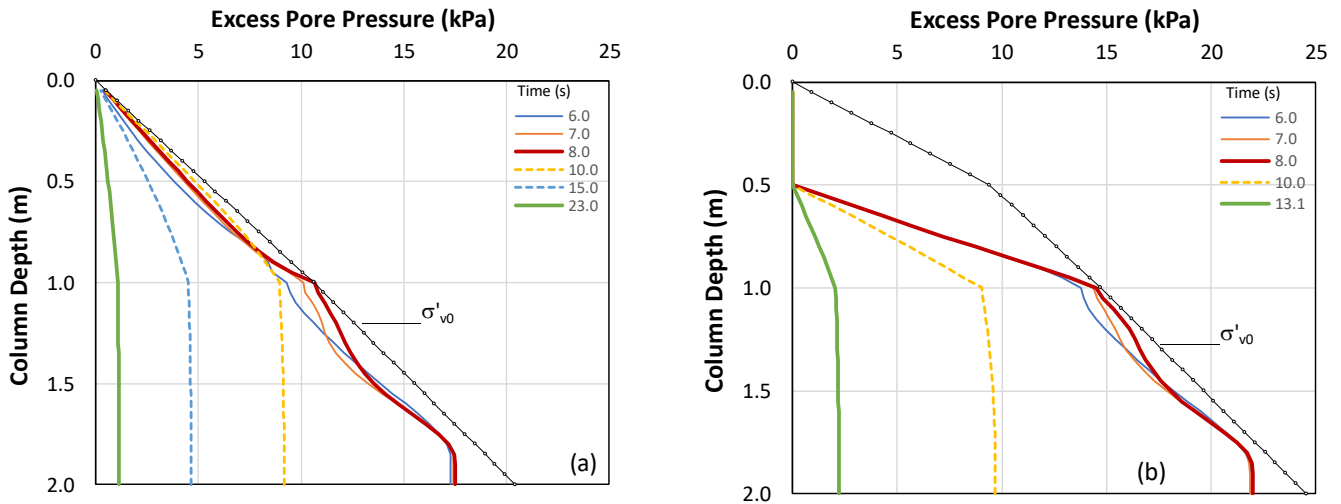Figure 9. Time history of ru for Case 2B subjected to GM1

Figure 10. Distribution with depth of EPP for (a) Case 2A and (b) Case 2B subjected to GM1

For Case 2A, r_u remained relatively high for a rather long time after the ground motion ended. Furthermore, the responses also varied at different depths, r_u of deeper observation points decreased faster than that of the middle ones. The responses of the shallower points increased after the ground motion stopped for 2 s, but r_u decreased. For Case 2B, r_u started to decrease immediately after time = 8 s and simultaneously for all depths.

The distribution of excess pore pressure (EPP) depth for Cases 2A and 2B, including the change with time, is shown in Figure 10. The EPP increased rapidly as the ground motion took place. The upper sand layer of Case 2A experienced a significant increase in EPP, but that of 2B remained constant, except near the boundary between upper and lower sand layers. For Case 2A, at time = 10 s, EPP in the lower sand layer decreased, but that in the upper layer increased, indicating an upward excess pore pressure flow. The further decrease in EPP was gradual, reaching an average r_u of 0.1 at time = 23 s, long after the ground motion was halted. For Case 2B, EPP decreased rapidly between time = 8 s and 13.1 s, reaching an average r_u of 0.1. This comparison suggests that the liquefied upper sand layer would cause the EPP dissipation of liquefied lower sand layer to be longer.

The time history of r_u for Case 2A subjected to GM2 is shown in Figure 11. The overall responses at different depths are shown in 11a, while r_u at selected depths for aftershock ground motion, starting at time = 15 s and ends at 17 s, is shown in b. It is highlighted that r_u at 15 s was not equivalent to zero as it had not been fully dissipated after the main shock.

The general responses r_u due to the aftershock were similar to those caused due to the main shock or GM1, and it remained relatively high for a rather long time after the ground motion ended. The responses r_u of deeper observation points decreased faster than the middle ones. Meanwhile, r_u of the shallower points increased after the ground motion ended in approximately 1.5 s and subsequently decreased.

The distribution of EPP depth and change of time is shown in Figure 11c. The average r_un at the start of the aftershock was approximately 0.39, and EPP increased rapidly immediately after this occurrence. At time = 19 s, EPP in the lower sand layer decreased, but in the upper layer, it increased slightly, indicating an upward excess pore pressure flow. The further decrease in EPP was gradual, reaching an average r_u of 0.1 at 31.5 s towards the end of the aftershock.
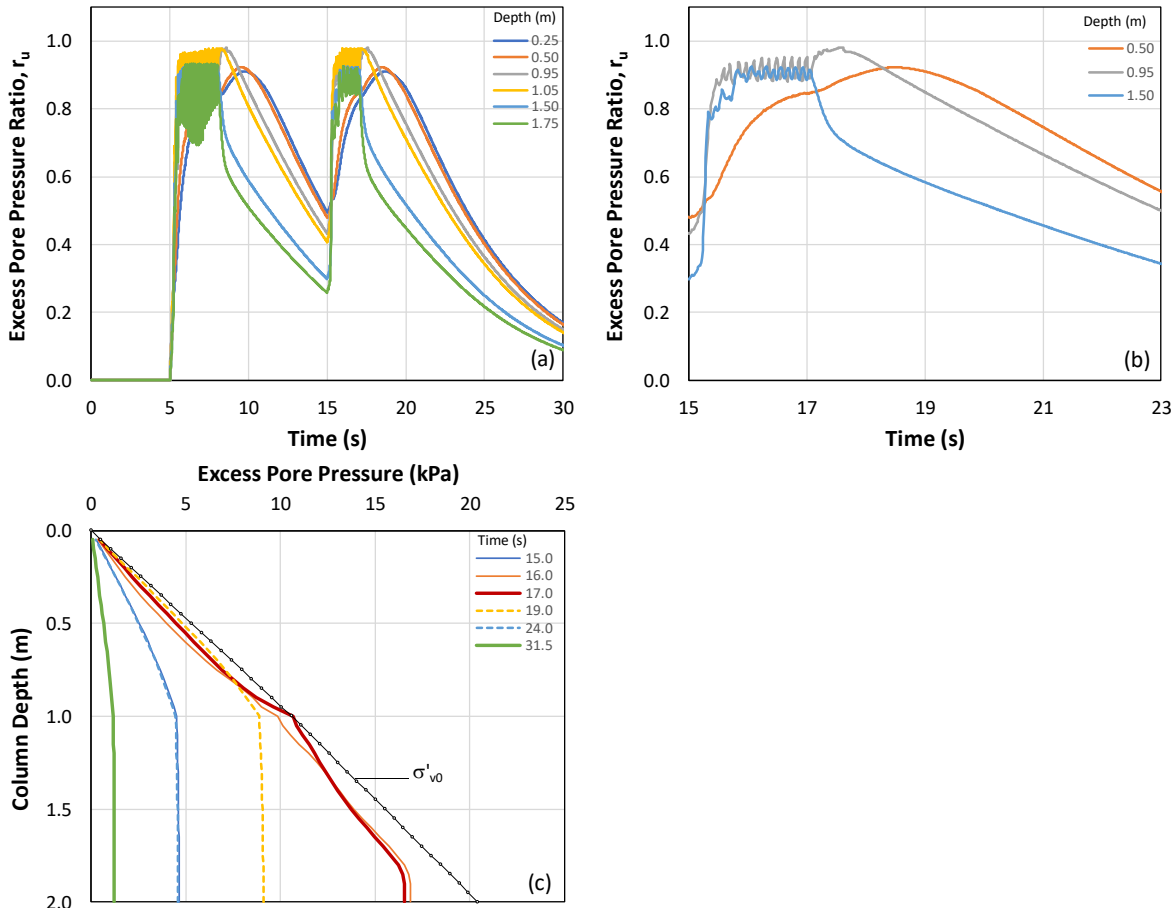
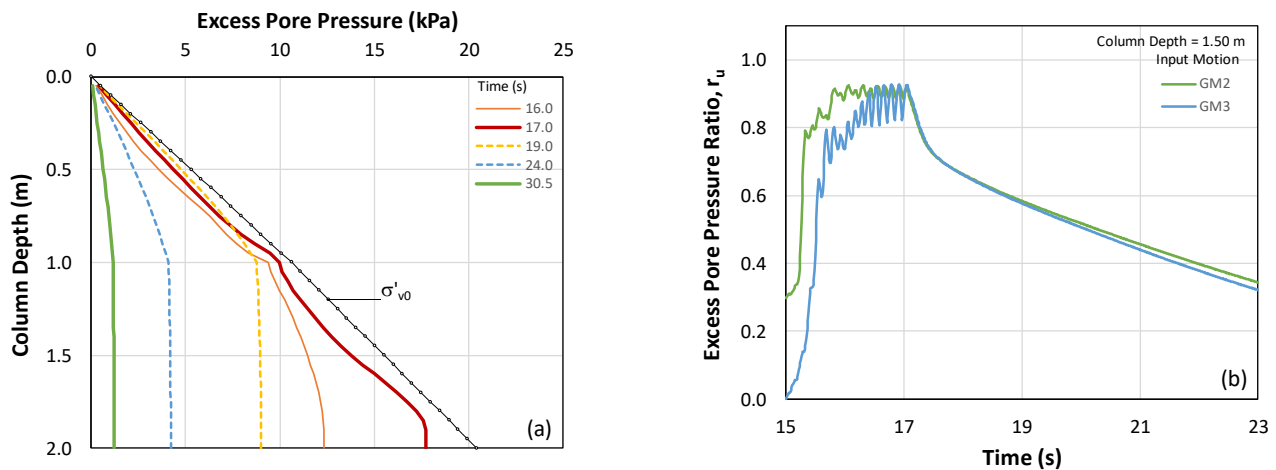Figure 11. Time history of ru and distribution with depth of EPP for Case 2A subjected to GM2

Figure 12. (a) Distribution with depth of EPP for Case 2A subjected to GM3, and (b) time history of ru comparison for smaller ground motion

The distribution of EPP with depth and change of time for Case 2A subjected to GM3 is shown in Figure 12a. By comparing Figures 12a to 10a (Case 2A subjected to GM1), the rate of increase in EPP was a function of ground motion amplitude, with the rise at 1 s after the start of

GM3 at 16 s less than that of GM1 at 6 s. The comparison between Figures 12a to 11c (Case 2A subjected to GM2) shows that the rate of decrease in EPP after the ground motion ended was quite similar, with the average r_u of 0.1 relatively achieved simultaneously. Figure 12b

compares the time history of r_u due to GM3 and GM2, indicating that the initial r_un at 15 s caused. its maximum to be reached more quickly, and therefore the state of liquefaction was lengthy.

4   DISCUSSION

The one-dimensional liquefaction numerical sand columns were adopted from the laboratory experiments of KK Model carried out by Kokusho and Kojima (2002). Qualitatively, it is imperative that the dynamic ESA results need to be validated. Case 1A is similar to KK Models 1 and 3, while 1B is similar to KK Model 2. The stepped EPP dissipation with depth similar to that of the seam for Case 1A was also observed in the laboratory tests KK Models 1 and 3. Its dissipation with depth for Case 1B is similar to that for KK Model 2. Cases 2A and 2B are similar to KK Models 2 and 4. The effect of lower groundwater level observed in Cases 2A and 2B were similar to that observed in KK Models 2 and 4, respectively.

The ground motion GM was used to capture the effect of aftershocks on EPP. The responses for Cases 1B and 2A subjected to this ground motion are shown in Figures 6a and 11a with increase and dissipation of EPP after the first motion as well as subsequent increase and dissipation after the second one. These responses are similar to those reported by Unjoh *et al.,* (2012), stating that the pore pressure measurements obtained from Nakashimo Station in a liquefied layer due to the 2011 earthquake off the Pacific Coast of Tohoku Earthquake showed the increase and dissipation of EPP after the first strong motion and subsequent increases after the second strong motion. The numerical results were able to capture the pattern of the field-measured pore pressure responses properly. In conclusion, the dynamic ESA model employed in this study represents the actual laboratory tests and field measurements.

The saturated sand layers in all the cases subjected to GM1 were liquefied, despite showing different EPP responses. All were liquefied at the end of the ground motion (time =

8 s), but the rate of EPP dissipation varied significantly. Case 1A achieved an average r_u of 0.1 at relatively 9 to 10 s, while 1B and 2A obtained the same average r_u at approximately 21 to 23 s, which are 13 to 15 s after the end of main shock ground motion. For Case 2B, with a deeper groundwater table and higher effective vertical stresses, the saturated sand layer was liquefied by the end of the ground motion as well, and the average r_un of 0.1 was achieved at relatively 13 s. The longer duration in Cases 1B and 2A appeared to be caused by the higher EPP in the upper sand layers, inhibiting the fast dissipation of EPP of the lower sand layers. The higher EPP in the upper sand layers was due to the upward seepage from the lower layers. All of these highlight the system response phenomenon suggested by Cubrinovski *et al.*, (2019).

Cases 1B and 2A subjected to GM2 were liquefied during both parts of the ground motion. The average r_u of 0.1 was achieved at approximately 30 s to 32 s, which are 13 to 15 s after the end of smaller aftershock ground motion or 22 s to 24 s after the main shock. A more detailed comparison of Cases 1B and 2A subjected to GM2 and GM3 suggested that the main shock would cause a longer liquefaction state during the aftershock.

The implication of the longer liquefaction state in the higher r_u state is based on the fact that a longer duration of lower shear strength conditions would exist. For sloping grounds, this would lead to a longer duration for lateral movement of the soil layers. Additionally, Cases 1A and 1B indicate how the coefficient of permeability of sand layers would affect the system response of the columns. Furthermore, 2A and 2B depict how the groundwater table affects the system response of the sand columns. All these suggest that the variability of geotechnical conditions plays an important role in the system response of the sand columns, and it needs to be incorporated further in liquefaction studies.

5 CONCLUSIONS

This numerical study assessed the effects of layered soils, variability, and aftershocks conditions on the liquefaction behavior of one-dimensional sand columns. Four sand columns with different geotechnical conditions were examined. The dynamic effective stress analyses were performed; the ESA employed the PM4Sand constitutive model implemented in the OpenSees platform and three sets of variable amplitude, single-frequency harmonic motions. It was found that the dynamic ESA model provided reasonable results with similar trends as observed in the laboratory tests and field measurements.

The following results are highlighted. First, the saturated sand layers in cases subjected to GM1 were liquefied with different detailed excess pore pressure (EPP) responses, highlighting the importance of the system's response. This is significantly influenced by the variation in the soil permeability coefficients. Second, the cases subjected to GM2 show a much longer, higher EPP state. A comparison between cases subjected to GM2 and GM3 indicated that a longer liquefaction state was observed during the aftershock. Lastly, the different EPP responses from the four sand columns proved that the variability of geotechnical conditions plays an important influence in the system response of liquefying soils.

The implication of the longer duration in the higher EPP is that a longer duration of lower shear strength conditions would exist. Additionally, the variability of geotechnical conditions needs to be explicitly examined in detailed liquefaction analyses.

DISCLAIMER

The authors declare no conflict of interest.

ACKNOWLEDGMENTS

REFERENCES

Andersen, K.H., Schjetne, K., 2013. Database of Friction Angles of Sand and Consolidation Characteristics of Sand, Silt, and Clay. *Journal of Geotechnical & Geoenvironmental Engineering*, 139(7): 1140-1155 (doi.org/10.1061/(ASCE)GT.1943-5606.0000839)

Boulanger, R., & Ziotopoulou, K., 2017. *PM4Sand (version 3.1): A Sand Plasticity Model for Earthquake Engineering Applications*. Davis, CA: Univ. of California.

Cubrinovski, M., Rhodes, A., Ntritsos, N., Van Ballegooy S., 2019. System response of liquefiable deposits. *Soil Dynamics and Earthquake Engineering*, 124:212–229 (doi.org/10.1016/ j.soildyn.2018.05.013)

Gallant, A.P., Montgomery, J., Mason, H.B., Hutabarat, D., Reed, A.N., Wartman, J., Irsyam, M., Simatupang, P.T., Alatas, I.M., Prakoso, W.A., Djarwadi, D., Hanifa, R., Rahardjo, P., Faizal, L., Harnanto, D.S., Kawanda, A., A., Himawan, A. & Yasin, W., 2020. The Sibalaya flowslide initiated by the 28 September 2018 MW 7.5 Palu-Donggala, Indonesia earthquake. *Landslides*, 17:1925–1934 (DOI: 10.1007/s10346-020-01354-1)

Harninto, D.S., & Prakoso, W.A., 2020. *Existence of Silt Seam Layer Triggering Flow Liquefaction on the Palu Mw 7.5 Earthquake 2018*. Melbourne, 10th International Conference on Geotechnique, Construction Materials and Environment.

Hutabarat, D. & Bray, J.D., 2021a. Effective Stress Analysis of Liquefiable Sites to Estimate the Severity of Sediment Ejecta. *Journal of Geotechnical & Geoenvironmental Engineering*, 147(5):04021024 (doi:10.1061/(ASCE)GT.1943-5606.0002503)

Hutabarat, D. & Bray, J.D., 2021b. Seismic Response Characteristics of Liquefiable Sites with and without Sediment Ejecta Manifestation. *Journal of Geotechnical & Geoenvironmental Engineering,* 147(6): 04021040 (doi.org/10.1061/(ASCE)GT.1943-5606.0002506)

Kokusho, T. & Kojima, T., 2002. Mechanism for Postliquefaction Water Film Generation in Layered Sand. *Journal of Geotechnical & Geoenvironmental Engineering,* 128(2):129-137 (doi:10.1061/(ASCE)1090-0241(2002)128:2(129))

Mason, H.B., Montgomery, J., Gallant, A.P., Hutabarat, D., Reed, A.N., Wartman, J., Irsyam, M., Simatupang, P.T., Alatas, I.M., Prakoso, W.A., Djarwadi, D., Hanifa, R., Rahardjo, P., Faizal, L., Harnanto, D.S., Kawanda, A., Himawan, A. & Yasin, W., 2021. East Palu Valley Flowslides Induced by the 2018 MW 7.5 Palu-Donggala Earthquake. *Geomorphology,* 373, pp. 107482 (doi:10.1016/j.geomorph.2020.107482)

Phoon, K.-K., Prakoso, W.A., Wang, Y., Ching, J., 2016, *Uncertainty Representation of Geotechnical Design Parameters*. In Reliability of Geotechnical Structures in ISO2394, Ed. K.K. Phoon, J.V. Retief, CRC Press.

Pramono, S., Prakoso, W.A., Cummins, P., Rahayu, A., Rudyanto, A., Syukur, F., Sofian, 2017. Investigation of Subsurface Characteristics by Using Parameters V_{s30}, HVSR and Combination of SPAC Method for Microtremor Array in Palu City and Surroundings. *International Journal of Technology* 8(6):983-992 (DOI: 10.14716/ijtech.v8i6.682)

Pramono, S., Prakoso, W.A., Rohadi, S., Karnawati, D., Santoso, E., Nurfajar, A., 2020. Influence of Seismicity Declustering on Ground Motion Prediction Equations for Central Sulawesi Seismic Region. *International Journal of Geomate* 19(71): 61 – 68 (DOI: 10.21660/2020.71.28369)

Prakoso, W.A., 2021. *Survei dan Kajian Geoteknik Gempa Palu 28 September 2018*. El-Markazi.

Rahayu, W., Nurizkatilah & Bahsan, E., 2020. *Analysis of Liquefaction Potential in Lolu Village, Palu Using SPT Method and Laboratory Test of Grain Size Distribution*. Bogor, International Seminar on Civil and Environmental Engineering. (doi:10.1088/1755-1315/622/1/012016)

Rahayu, W., Yuliyanti, I. & Bahsan, E., 2020. *Analysis of Potential Liquefaction Using Cone Penetration Test Data and Grain Size Distribution Test with Case Study of Liquefaction in Lolu Village*. Bogor, International Seminar on Civil and Environmental Engineering. (doi:10.1088/1755-1315/622/1/012015)

Ramdhiani, E., Prakoso, W.A., 2020. *Cyclic Behaviour of Palu Sandy Soils in Cyclic Simple Shear Test*. Solo, 7th International Conference on Engineering, Technology, and Industrial Application. (DOI: 10.1088/1742-6596/1858/1/012039)

Unjoh, S., Kaneko, M., Kataoka, S., Nagaya, K., Matsuoka, K., 2012. Effect of Earthquake Ground Motions on Soil Liquefaction, *Soils and Foundations,* 52(5):830–841 (DOI: 10.1016/j.sandf.2012.11.006).

You, T.L., et al., 2001. Liquefaction Resistance of Soils: Summary Report from the 1996 NCEER and 1998 NCEER Workshops on Evaluation of Liquefaction Resistance of Soils, *Journal of Geotechnical & Geoenvironmental Engineering,* 127(10): 817–833 (DOI: 10.1061/(ASCE)1090-0241(2001)127:10(817).